Journal of Applied Physics

RESEARCH ARTICLE | APRIL 01 2024

Epitaxial growth and characterization of (110)-oriented YBCO/PBCGO bilayer and YBCO/PBCGO/YBCO trilayer heterostructures

Hom Kandel ; Nathan Arndt ; Zhongrui Li ; Jungwoo Lee; Yuchuan Yao; Susmita Roy; Hillary Cunliffe-Owen; Dmitry Reznik ; Chang-Beom Eom

Check for updates

J. Appl. Phys. 135, 135301 (2024)
https://doi.org/10.1063/5.0195242

View Online
Export Citation

01 April 2024 20:16:50

AIP Publishing

Journal of Applied Physics ARTICLE pubs.aip.org/aip/jap

Epitaxial growth and characterization of (110)-oriented YBCO/PBCGO bilayer and YBCO/PBCGO/YBCO trilayer heterostructures

Cite as: J. Appl. Phys. **135**, 135301 (2024); doi: 10.1063/5.0195242
Submitted: 31 December 2023 · Accepted: 17 March 2024 ·
Published Online: 1 April 2024

View Online Export Citation CrossMark

Hom Kandel,[1,a)] Nathan Arndt,[1] Zhongrui Li,[2] Jungwoo Lee,[3] Yuchuan Yao,[3] Susmita Roy,[4] Hillary Cunliffe-Owen,[1] Dmitry Reznik,[4] and Chang-Beom Eom[3]

AFFILIATIONS

[1]Applied Physics Laboratory, University of Wisconsin-Parkside, Kenosha, Wisconsin 53144, USA
[2]Electron Microbeam Analysis Laboratory, University of Michigan, Ann Arbor, Michigan 48109, USA
[3]Department of Materials Science and Engineering, University of Wisconsin-Madison, Madison, Wisconsin 53706, USA
[4]Department of Physics, University of Colorado Boulder, Boulder, Colorado 80309, USA

[a)]**Author to whom correspondence should be addressed:** kandel@uwp.edu

ABSTRACT

We have grown and characterized (110)-oriented $YBa_2Cu_3O_{7-x}$ (YBCO)/$PrBa_2(Cu_{0.8}Ga_{0.2})_3O_{7-x}$ (PBCGO) bilayer and YBCO/PBCGO/YBCO trilayer heterostructures, which were deposited by pulsed laser deposition technique for the nanofabrication of (110)-oriented YBCO-based superconductor (S)/insulator (I)/superconductor (S) tunneling vertical geometry Josephson junction and other superconductor electronic devices. The structural properties of these heterostructures, investigated through various x-ray diffraction techniques (profile, x-ray reflectivity, pole figure, and reciprocal mapping), showed (110)-oriented epitaxial growth with a preferred c-axis-in-plane direction for all layers of the heterostructures. The atomic force microscopy measurement on the top surface of the heterostructures showed crack-free and pinhole-free, compact surface morphology with about a few nanometer root mean square roughness over the $5 \times 5\,\mu m^2$ region. The electrical resistivity measurements on the (110)-direction of the heterostructures showed superconducting critical temperature (T_c) values above 77 K and a very small proximity effect due to the interfacial contact of the superconducting YBCO layers with the PBCGO insulating layer. Raman spectroscopy measurements on the heterostructures showed the softening of the A_g-type Raman modes associated with the apical oxygen O(4) and O(2)-O(3)-in-phase vibrations compared to the stand-alone (110)-oriented PBCGO due to the residual stress and additional two Raman modes at ~600 and ~285 cm^{-1} frequencies due to the disorder at the Cu–O chain site of the PBCGO. The growth process and structural, electrical transport, and Raman spectroscopy characterization of (110)-oriented YBCO/PBCGO bilayer and YBCO/PBCGO/YBCO trilayer heterostructures are discussed in detail.

© 2024 Author(s). All article content, except where otherwise noted, is licensed under a Creative Commons Attribution (CC BY) license (https://creativecommons.org/licenses/by/4.0/). https://doi.org/10.1063/5.0195242

01 April 2024 20:16:50

I. INTRODUCTION

Thin film growth and optimization of the structural and electrical properties of the multilayer heterostructures are vital for developing many superconductor electronic devices such as Josephson junctions, three-terminal devices, and integration of complex circuits such as flux transformers, interconnects, ground planes, and multichip modules.[1–5] High critical temperature (T_c) superconductor (S) $YBa_2Cu_3O_{7-x}$ (YBCO) based heterostructures are developed for both device applications and basic science research, such as the studies of mechanisms for high T_c superconductivity, 2D/3D superconductivity, and measurement of correlation energy. These heterostructures typically have the superconductor /dielectric/superconductor, superconductor/normal metal/superconductor, and superconductor/insulator (I)/superconductor geometry, with the middle layer as the isolation layer, normal metal, or the insulator. Of particular interest are YBCO-based S/I/S tunneling sandwich-type Josephson junctions, which could operate in low-cost liquid nitrogen (77 K) systems as

© Author(s) 2024

opposed to expensive and complex liquid helium (4.2 K) systems. In addition, these junctions may have I_cR_n products (with I_c being the junction critical current and R_n being the normal resistance) at least one order of magnitude larger than in the conventional low-temperature superconducting (LTS) junctions,[6] offering the possibility of their applications in superconductor quantum interference device (SQUID) magnetometers, rapid single flux quantum (RSFQ) circuits, and terahertz (THz) frequency devices[7–16] (THz transmitters/receivers and THz superconducting metamaterials for sensing, ultrasensitive bolometer and active THz beamforming, steering, and switching for 6G communication network), which cover in the frequency range from 0.1 to 30 THz (3.3–1000 cm^{-1} in wavenumber and 3 mm to 10 μm in wavelength). The main differences between LTS and YBCO are that the superconducting gap magnitude is much larger for YBCO (e.g., the superconducting gap of YBCO is greater than 40 meV compared to ~1.5 meV in LTS niobium) and YBCO still has residual conductivity at relatively high frequencies even at temperatures much lower than T_c. The lower energy gap in LTS, such as the ~1.5 meV in niobium, imposes an upper-frequency cutoff of only about 0.75 THz.[8,9] Although the YBCO junctions have proven to be efficient tools for low-power applications, such as the study of properties of bolometers,[10–12] their radiation power range is still low. The fabrication of YBCO Josephson junctions in the layered structure such as the vertical/sandwich-type geometry may enhance radiation power because of their different geometries and capacitance powers.

Fabrication of YBCO-based Josephson junctions in the step-edge/ramp-type or sandwich/vertical-type geometry has been reported by some research groups.[17–22] However, these junctions had T_c values below the liquid nitrogen boiling temperature (77 K), possessed a small figure of merit (I_cR_n product), and were unreproducible. YBCO junctions are also fabricated on bicrystal substrates, which require rather expensive substrates and also have restrictions on the junction geometry. The sandwich-type is the standard design applied in the fabrication of LTS Josephson junctions such as the S/I/S sandwich-type Nb/AlO_x/Nb junctions. This type of design provides mechanical stability and higher density in the superconducting devices compared to the ramp-type junctions, thus allowing an opportunity to fabricate more junctions per unit volume.

The nanofabrication of the YBCO-based S/I/S sandwich-type (vertical geometry) Josephson junction requires high epitaxial-quality superconducting YBCO films at the top and bottom and about a nanometer-thick insulating layer in between due to the small coherence length (~1.2 nm along ab-plane and 0.5 nm along the c-axis) of the YBCO. In addition, the middle insulating layer must be structurally compatible and chemically stable with the YBCO superconducting layers at the processing temperature of superconducting thin films and also must have a high electrical resistivity to provide enough potential barrier in the junction device. Moreover, further complications arise concerning the superconductivity of the films and the interfacial properties of the bottom and top YBCO layers with the middle insulating layer. Therefore, fabricating S/I/S heterostructures with high critical current (T_c), high critical current density (J_c), and very small or no proximity effect is vital for the realization of the reproducible YBCO-based S/I/S sandwich-type Josephson junction and other superconductor electronic devices with high figure of merit.

In our previous work, we have demonstrated that (110)-oriented PBCGO may serve as the effective insulating layer in the YBCO-based S/I/S type Josephson junction device in (110)-orientation.[23] In this work, we have deposited (110)-oriented YBCO/PBCGO and (110)-oriented YBCO/PBCGO/YBCO vertical bilayer and trilayer heterostructures using the pulsed laser deposition (PLD) technique. The as-grown heterostructures were investigated in terms of structural, electrical transport, and Raman scattering properties. The objective was to optimize their structural and electrical transport properties for the nanofabrication of the (110)-oriented YBCO-based vertical, trilayered Josephson junction device. Vertical trilayers offer a straightforward geometry that is ideal for integration into the peripheral circuits by providing a clearly defined junction area, and in principle, epitaxial barrier layers of fixed thicknesses.[24] Moreover, the vertical geometry allows the flow of the electric current along the CuO_2 planes across the junctions, which is the direction of the larger coherence length and the current density. PLD is a powerful and well-established technique in fabricating YBCO and PBCGO-based heterostructures since the deposition rate is relatively higher than in other vacuum deposition techniques such as sputtering or co-evaporation. Here, we discuss the growth process, structural, electrical transport, and Raman spectroscopy measurement and analysis of bilayered and trilayered cuprate heterostructures.

II. EXPERIMENTAL

We deposited (110)-oriented YBCO/PBCGO and (110)-oriented YBCO/PBCGO/YBCO heterostructures on (110)-oriented $LaAlO_3$ using the standard PLD technique. A KrF excimer laser with 248 nm wavelength, 3 Hz repetition rate, and 1.5 J/cm^2 energy density was used to ablate the high-density (5.94 gm/cm^3) discs of YBCO and PBCGO inside a chamber that was vacuumed to 5×10^{-7} Torr. The distance between ablation targets and substrate was kept at 4 cm, and the heterostructures were deposited in an oxygen atmosphere at a pressure of 200 m Torr. The thin film growth parameters were similar for YBCO and PBCGO except for the growth temperatures. We deposited the YBCO thin film on top of the YBCO template (buffer) layer and the PBCGO thin film on top of the PBCGO template (buffer) layer. We started fabricating the bilayer heterostructure by depositing a YBCO template layer on the (110)-LAO substrate at 600 °C. Afterward, the substrate temperature was raised to 710 °C for the deposition of the YBCO film. Subsequently, a PBCGO buffer layer was deposited on top of the YBCO film at 625 °C, followed by the deposition of the PBCGO thin film by raising the substrate temperature to 725 °C. To grow a trilayer heterostructure, an additional YBCO layer was deposited on top of the intermediate PBCGO layer repeating the same process applied for the deposition of the bottom YBCO layer on top of the LAO substrate. After the completion of each layer growth, annealing was performed at 500 °C in oxygen gas at one atmospheric pressure for 1 h.

X-ray diffraction measurements of the mono-layer, bi-layer, and tri-layer heterostructure samples were performed in a Bruker D8 General Area Detector Diffraction System (GADDS) using Cu K_α x-ray radiation. The atomic force microscopy (AFM)

01 April 2024 20:16:50

© Author(s) 2024

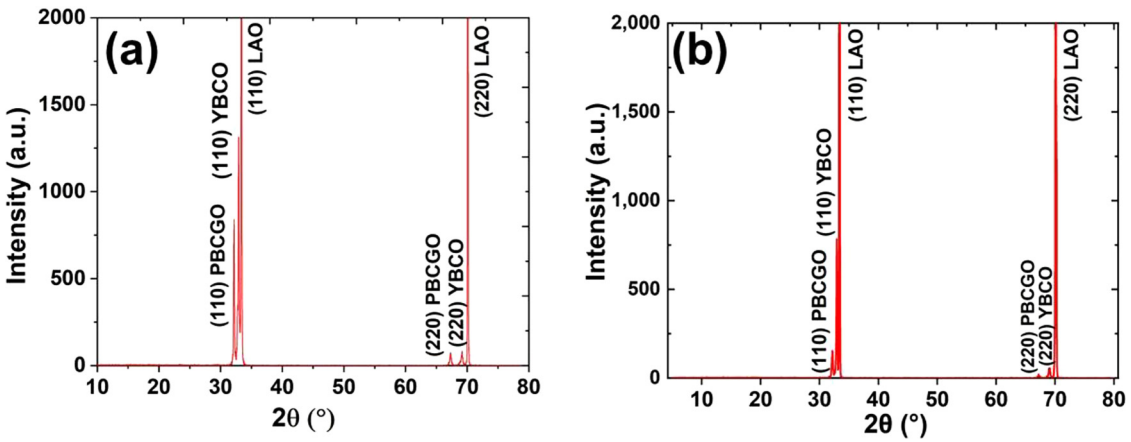

FIG. 1. X-ray diffraction pattern of (a) (110)-oriented YBCO/PBCGO; (b) (110)-oriented YBCO/PBCGO/PBCGO deposited on the (110)-oriented $LaAlO_3$ (LAO) substrate.

measurement of the heterostructure was performed in a Bruker's MultiMode 8-HR atomic force microscope in the tapping mode to study the surface morphology of the heterostructures. Electrical resistivity measurements were performed in a liquid helium cryostat using the standard DC four-probe technique.

Raman spectra were measured using a 532 nm solid-state laser with a power of 29 mW at room temperature with the help of a single-stage McPherson spectrometer equipped with a liquid nitrogen-cooled charge-coupled device (CCD) detector. We used 1800 grooves/mm grating for better resolution. The entrance slit of the spectrometer was opened to 0.15 mm to avoid chromatic aberrations of the collecting optics. The spectra were taken with parallel scattering configurations zz and *x'x'*, which indicate that both the incident and scattered light polarizations were parallel to the (0 0 1) and ($\bar{1}$10) directions, respectively.

III. RESULTS AND DISCUSSION

A. Structural characterization

The film orientation and phase purity of the single film and heterostructures were examined by x-ray diffraction (XRD) measurements. The 2θ/θ XRD patterns of YBCO/PBCGO and YBCO/PBCGO/YBCO heterostructures indicated (110)-epitaxy without any detectable second phases. Figures 1(a) and 1(b) show only two sets of distinct peaks, with the first set of peaks representing the (110) PBCGO, (110) (YBCO), and (110) LAO, and the second set of peaks representing the (220) PBCGO, (220) (YBCO), and (220) LAO, respectively. Based on the 2θ diffraction angles for (110) peaks in the graph, the *interplanar d-spacing* (d_{110}) values for (110)-oriented PBCGO and (110)-oriented (YBCO) are equivalent to 0.2776 and 0.2725 nm, respectively.

X-ray reflectivity (XRR) was performed on (110)-oriented YBCO to calibrate the thickness of the heterostructure samples. Based on the XRR data, the total thickness of the (110)-oriented YBCO/PBCGO heterostructure was estimated to be 167 nm with a 67 nm thick PBCGO layer on top of the 100 nm YBCO layer. Likewise, the total thickness of the (110)-oriented YBCO/PBCGO/YBCO trilayered heterostructure was estimated to be 260 nm with 100 nm for each bottom and top YBCO layer and 60 nm for the middle PBCGO layer.

Figure 2 displays the (110) pole figure of the YBCO (bottom)/PBCGO (top) heterostructure. The center of the pole figure is the orientation of (110), which is at 2θ = 32.14 ° in the XRD pattern and is surrounded by the isolated (101), (10$\bar{1}$), (01$\bar{1}$), and (011) orientations, suggesting that the top PBCGO layer is a single crystalline. Compared to undoped $PrBa_2Cu_3O_{7-x}$ (PBCO) PBCO, there are also no new x-ray diffraction peaks on the PBCGO film. This suggests that the Ga atoms substituted Cu ions on PBCO, instead

01 April 2024 20:16:50

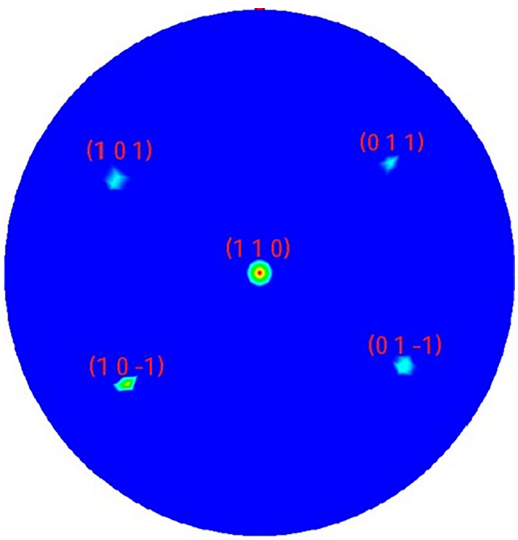

FIG. 2. X-ray (110) pole figure plot of the YBCO (bottom)/PBCGO (top) heterostructure deposited on (110)-oriented LAO substrate.

© Author(s) 2024

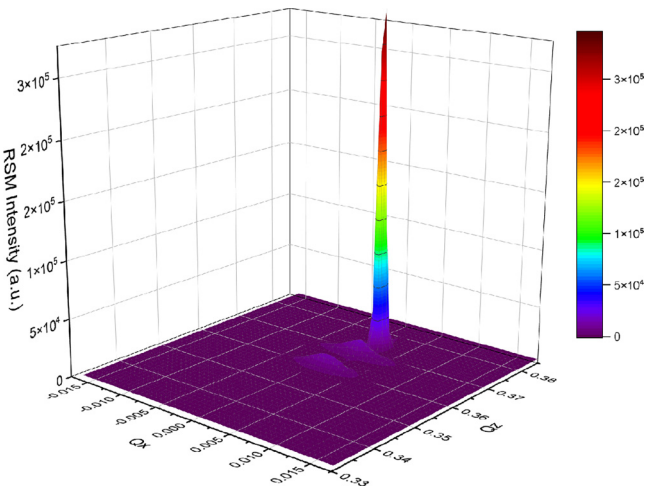

FIG. 3. Reciprocal space mapping (RSM) of the (110)-oriented YBCO (bottom)/PBCGO (top) heterostructure deposited on the LAO (110) substrate.

of sitting at any interstitial position, which would cause a scattering phase shift and lead to new diffraction peaks. The diffraction intensity can be expressed in the following equation as the structure factor times its conjugate:

$$I \sim F^{*}_{hkl} \cdot F_{hk\ell}, \tag{1}$$

where the structure factor $F_{hk\ell}$ is the vector sum of waves scattered by all atoms within the unit cell and (h,k,l) are the Miller indices in the real-space plane.[25] The structure factor as expressed in the following equation,

$$F_{hk\ell} = \sum_{j=1}^{N} f_j e^{[-2\pi i(hx_j + ky_j + \ell z_j)]}, \tag{2}$$

is proportional to the atomic scattering factor (f_j, charge of the *jth* element in the unit cell) in which x_j, y_j, z_j are the positional coordinates of the *jth* atom, and N refers to all atoms in the unit cell.[26]

Figure 3 shows the reciprocal space map of the (110)-oriented YBCO (bottom)/PBCGO (middle)/YBCO (top) heterostructure deposited on the (110)-oriented LAO substrate. Reciprocal space mapping (RSM) is a method to determine the crystallographic orientation and structure of the crystalline material by mapping the reciprocal space of crystals, which is essentially the Fourier transform of the real-space crystal lattice. The reciprocal map can be analyzed to determine the crystallographic orientation of the sample including the information about the orientation of crystal grains, any preferred orientation (texture) in the material, and the crystal symmetry. Additionally, the intensity and shape of the diffraction spots can be used to extract information about the crystal structure, such as lattice parameters and the presence of defects. In our measurement, we saw three Q_z vector peaks corresponding to (110) LAO, (110) YBCO, and (110) PBCGO, respectively, where (110) LAO had the highest intensity. This is consistent with the intensities on the XRD profile of the heterostructure on the LAO substrate. Similar to the pole figures, the reciprocal mapping of the heterostructure sample revealed the texture of the individual layers to be crystallographic unique orientation distributed within the sample. This information is crucial for predicting heterogeneous junction properties.

B. Morphological characterization

The single films or multilayered heterostructures must be crack-free for many superconducting device applications. A prominent feature of the (110)-oriented YBCO and YBCO/PBCO films

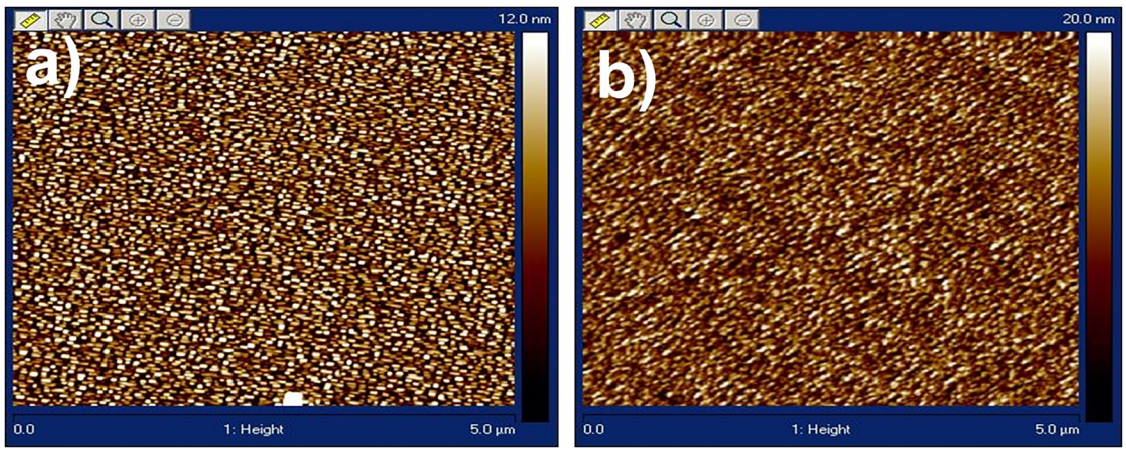

FIG. 4. AFM Surface images of (a) (110)-oriented YBCO (100 nm/PBCGO(67 nm) and (110)-oriented YBCO (100 nm)/PBCGO (60 nm)/YBCO (100 nm) heterostructures deposited on the (110)-oriented LAO substrate.

01 April 2024 20:16:50

© Author(s) 2024

grown on (110)-oriented $SrTiO_3$ (STO) substrate was that they typically contained cracks.[27] As shown in Fig. 4, the AFM surface measurements showed the top surfaces of both heterostructures without any cracks, pinholes, secondary outgrowths, or other defects. The root mean square surface roughness values in the $5 \times 5\,\mu m^2$ region of YBCO (100 nm)/PBCGO (67 nm) bilayered heterostructure and (110)-oriented YBCO (100 nm)/PBCGO (60 nm)/YBCO (100 nm) trilayered heterostructure were measured ~2 and ~3 nm, respectively.

We adopted the following strategies to obtain smoother surface morphology and prevent the occurrence of pinholes, secondary outgrowths, and other defects from the surface of the films.

(1) Substrate preparation: the substrates were annealed with oxygen at 1000 °C for 9 h, which effectively formed atomically flat single-terminated surfaces, reducing the overall surface roughness. The substrates were then cleaned thoroughly with acetone and isopropyl alcohol, followed by drying with nitrogen gas. (2) Precursor/oxide powder purity: high-quality precursor materials (oxide powders) with high purity levels (99.99%) were used to fabricate bulk YBCO and PBCGO powder and discs (targets) since the impurities in the precursors/ingredients can lead to pinholes, secondary outgrowths, and other defects. (3) Optimized deposition technique: we employed a pulsed laser deposition technique that provided uniform coverage and minimized defects compared to other thin film deposition techniques. (4) Controlled deposition parameters: we conducted several experiments to optimize these growth parameters such as the substrate temperature, oxygen pressure inside the deposition chamber, pulsed laser energy and repetition rate, and growth rate, which helped us to minimize pinholes and other film defects. (5) Growth of template (buffer) layer: depositing a YBCO template (buffer) layer on top of the LAO substrate improved the quality of the YBCO film by providing a smoother surface and reducing the diffusion of defects from the substrate. (6) Post-deposition annealing: The annealing process after the film deposition enhanced the oxygenation of the YBCO and PBCO films while reducing the defects in the films. Annealing helped recover small defects and improve the overall quality of the YBCO and PBCGO films.

C. Electrical transport characterization

Figure 5 shows the temperature-dependent electrical resistivity measurements on the (110)-oriented YBCO single layer, (110)-oriented YBCO/PBCGO bilayer, and (110)-oriented YBCO/PBCGO/YBCO tri-layer samples. While the onset T_c values of single-layer (110)-oriented YBCO, (110)-oriented YBCO/PBCGO

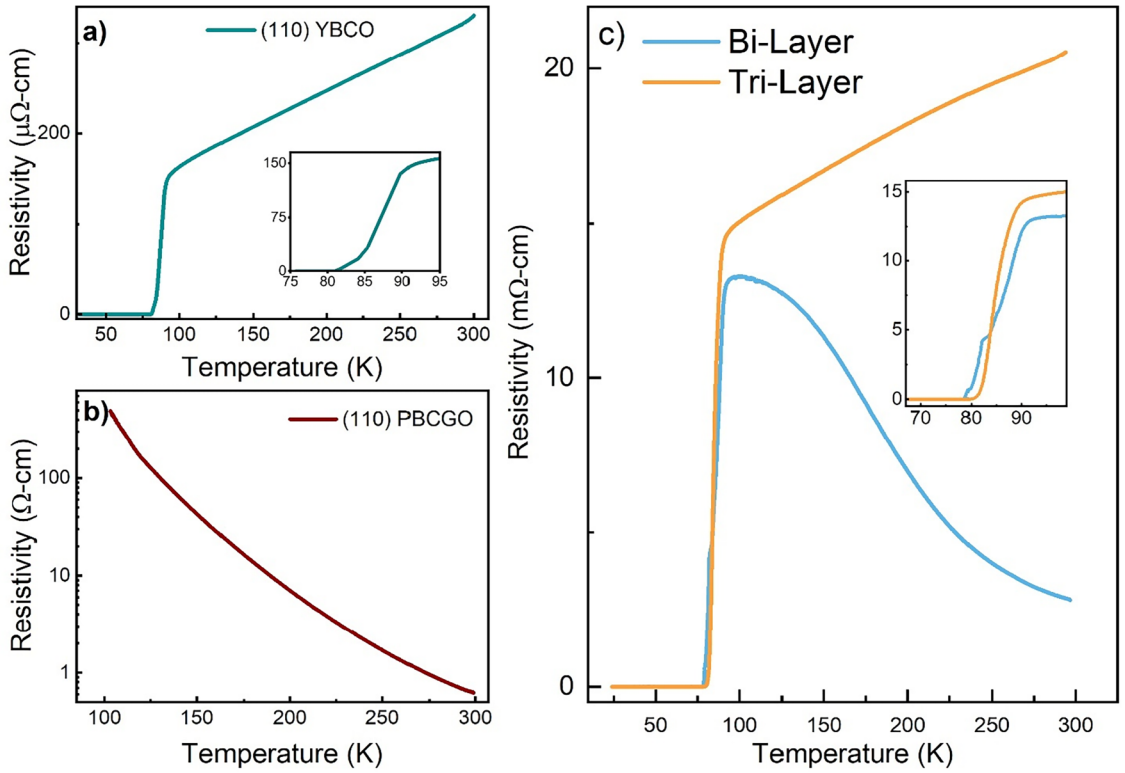

FIG. 5. Plot of electrical resistivity vs temperature for (a) (110)-oriented YBCO mono-layer (100 nm), (b) (110)-oriented PBCGO mono-layer (100 nm), and (c) (110)-oriented YBCO (100 nm)/PBCGO (67 nm) bi-layer and (110)-oriented YBCO (100 nm)/PBCGO (60 nm)/YBCO (100 nm) tri-layer heterostructure.

01 April 2024 20:16:50

© Author(s) 2024

bilayer, and (110)-oriented YBCO/PBCGO/YBCO tri-layer samples are equivalent to ~94.5, ~93, and 94 K, respectively, their T_c (0) values are equivalent to ~81.5, ~80.5, and ~79 K, respectively. These values are in close agreement with the (110)-oriented YBCO/PBCO multilayers in the literature.[28–30] The lower T_c (0) values of bilayer and trilayer samples compared to the single-layer YBCO sample indicated a small proximity effect due to the interfacial contact of the insulating PBCGO with the superconducting YBCO.

We also observed relatively lower T_c (0) values in our all samples. The (110)-oriented YBCO thin films have been found with lower T_c (0) values than the c-axis films in the literature.[28–31] There have been numerous reports on *c*-axis oriented films with a T_c (0) of 90 K or above while (110)-oriented films with lower than 90 K. One reason for the relatively lower T_c (0) values of our single and multilayers compared to the c-axis single-layer YBCO is due to the low oxygen content of the samples,[32,33] i.e., the oxygen content of our samples $YBa_2Cu_3O_{7-x}$ and $PrBa_2(Cu_{0.8}Ga_{0.2})_3O_{7-x}$ is 6.9. This is less than the oxygen content in the fully oxygenated samples, which is 7. If oxygen was taken into the film and diffused sufficiently deep inside the film during the thin film growth process, the YBCO film would have a high zero-resistance temperature, T_c (0). Thus, the realization of YBCO thin films with high T_c (0) depends on the oxygen content absorbed.[32,33] The other reason for the lower T_c (0) is due to the characteristic property of the (110)-orientation, which usually yields relatively lower T_c (0) values compared to the c-axis counterparts due to the low growth temperature of the (110)-oriented cuprate films, which causes the degradation of the superconducting properties in the YBCO films as indicated by the small T_c (0).[27]

D. Raman spectroscopy measurement

In our Raman spectroscopy measurement on the (110) YBCO/(110) PBCGO heterostructure, we observed two prominent A_g-type Raman modes[23,34–36] at 409 and 482 cm^{-1}, associated with O(2)–O(3) in-phase and O(4) apical oxygen vibration along the c-axis of PBCGO, respectively (see Fig. 6). However, these Raman modes have softened in the heterostructure compared to the standalone (110)-oriented PBCGO.[23,34,35] This seems to be the effect of the residual stress on the top PBCGO thin film as the frequency shift of the Raman peak is proportional to the stress.[37] When a thin film is subjected to stress, the lattice structure and lattice vibration will change, leading to a shift in the Raman peaks. The stress on the top surface of the PBCGO was induced as a result of the structural variation and the thermal misfit between the YBCO and LAO substrate and the PBCGO and YBCO thin films. In addition, we observed two Raman modes at ~600 and ~285 cm^{-1} frequencies, associated with the oxygen vibration at the Cu–O chain site of PBCGO. While these two Raman modes are absent in the Raman spectroscopy of undoped PBCO, they appear in the infrared (IR) spectroscopy of PBCO. The Raman peaks appeared in the PBCGO due to the broken symmetry at the Cu–O chain site after the partial doping of Ga with Cu in PBCO.[23,34,35]

Thus, we fabricated excellent epitaxial-quality (110)-oriented YBCO/PBCGO bilayer and YBCO/PBCGO/YBCO trilayer heterostructures with excellent surface morphology. One of the features

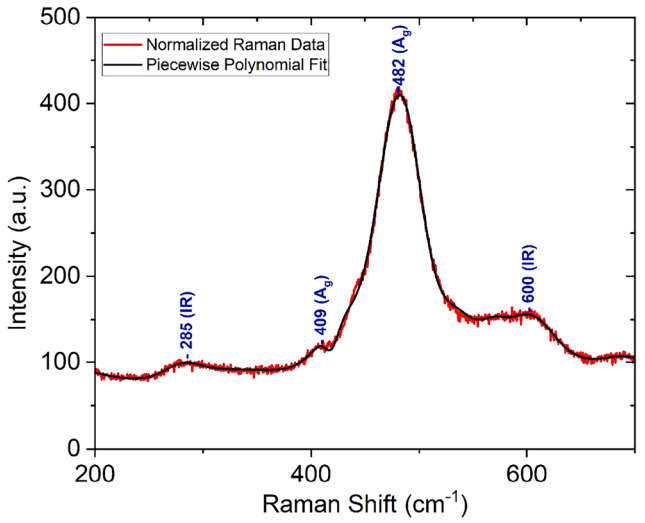

FIG. 6. Room temperature zz (c-axis) polarized Raman spectra of 167 nm thick (110)-oriented YBCO (100 nm)/PBCGO (67 nm) measured by 532 nm laser excitation. The black color solid line represents the third-degree polynomial fit for the normalized Raman data (red color).

of our (110)- oriented YBCO and PBCGO thin film growth process was the predeposition of the YBCO and PBCGO template (buffer) layers, respectively, contrary to the growth of the PBCO template layer, which tends to nucleate in (110) orientations at temperatures below 100 °C, usually used for growing c-oriented or (103)-oriented films.[38,39] On the other hand, the (110)-films grown at low temperatures have low T_c (0) values. However, by introducing the buffer layer growth before the actual thin film growth at the raised temperature, one can enhance the T_c (0) values on (110)-orientation. Our growth technique can be further improved by combining the thin film growth process with *in situ* monitoring techniques such as RHEED (Reflection High Energy Electron Diffraction) or optical spectroscopy to monitor the growth process in real time and adjust parameters accordingly to minimize pinhole and defect formation. Protective layers can be implemented on top of the YBCO film to shield it from external contaminants and prevent pinhole formation due to environmental factors. Using high-density ceramic discs (targets) for the laser ablation can help to reduce or prevent the secondary outgrowths on the surface morphology. Optimizing the thickness of the films while still maintaining superconducting properties can help reduce the occurrence of pinholes as thicker films are more prone to defects like pinholes. Since smooth surfaces are crucial for the reliability and large-scale yield of the fabrication process of multilayers in YBCO-based electronic devices, smoothing of the thin film layers using new cutting-edge surface smoothing techniques such as the ion cluster beam bombardment followed by annealing in the ambient oxygen may be useful for the subsequent homo- or heteroepitaxial multilayer thin film growth.[40]

Usually, YBCO-based devices have been fabricated on either single- or bi-crystal $SrTiO_3$ (STO), $LaAlO_3$ (LAO), MgO, and

01 April 2024 20:16:50

© Author(s) 2024

$LaSrGaO_4$ (LSGO) substrates with excellent superconducting properties. These substrates are very compatible with YBCO thin film in terms of their lattice constants and thermal expansion coefficients. Other substrates for YBCO film deposition are Si wafers, which are relatively cheaper, come in larger areas, and specifically offer the possibility for ultrahigh frequency (THz) detectors and RF electronic applications.[41] However, the deposition of the YBCO thin film directly on the Si wafer is not possible because of a mismatch in the lattice constants and thermal expansion coefficients between YBCO and Si. Another problem is the diffusion of Ba atoms into Si during the high-temperature growth of YBCO crystal. To overcome this problem, the YBCO film can be deposited on top of the CeO_2/YSZ ($Y_2O_3 + ZrO_2$) buffer layer/Si substrate.[41] Although in this work, we utilized LAO as the substrate, our technology can be scaled by depositing our bilayer and trilayer heterostructures on top of the CeO_2/YSZ/Si template layer for the development of good-quality terahertz frequency devices. These devices may allow us to overcome two main limitations affecting metallic metamaterial resonating in the terahertz (THz) range: ohmic losses and tunability of their optical response, offering the potential application in THz emitters and receivers.[7–16,41,42]

IV. CONCLUSIONS

We investigated the structural, electrical transport and Raman spectroscopy properties of the (110)- oriented YBCO/PBCGO bilayer and YBCO/PBCGO/YBCO trilayer heterostructures deposited on (110)-oriented LAO substrates using PLD technique. X-ray diffraction measurements (profile, XRR, pole figure, and reciprocal mapping) of YBCO/PBCGO bilayer and YBCO/PBCGO/YBCO trilayer heterostructures showed (110)-oriented epitaxial growth with a preferred *c-axis-in-plane* direction for all the thin film layers of the heterostructure. We observed a crack-free and pinhole-free compact surface morphology with about a few nanometer root mean square roughness over the $5 \times 5\,\mu m^2$ region on the top surface of bilayered and trilayered heterostructures. The electrical resistivity measurements on the (110)-direction of the bilayered and trilayered heterostructures showed their T_c (0) values around 80 K with a small proximity effect due to the interfacial contact of YBCO and PBCGO in the heterostructures. We found the softening of the prominent A_g-type Raman modes associated with the apical oxygen O(4) and O(2)-O(3)-in-phase vibrations compared to the stand-alone (110)-oriented PBCGO due to the residual stress on the top surface due to the underlying YBCO layers and the LAO substrate. In addition, two disorder-related Raman modes appeared at ~600 and ~285 cm^{-1} frequencies in the spectrum due to the presence of Ga at the Cu–O chain site of the PBCGO. It is worth noting that our technology can be scaled by depositing cuprate heterostructures on top of the CeO_2/YSZ/Si template layer for the development of good-quality terahertz frequency devices.

ACKNOWLEDGMENTS

This work was supported, in part, by WiSys and UW System Applied Research under Grant No. 102-4-812000-AAH1775 (2019–2021), CNHS Summer Research Award (2022–2023), and URAP award (2022–2023).

AUTHOR DECLARATIONS

Conflict of Interest

The authors have no conflicts to disclose.

Author Contributions

Hom Kandel: Conceptualization (lead); Data curation (equal); Formal analysis (equal); Funding acquisition (lead); Investigation (equal); Project administration (equal); Writing – original draft (equal); Writing – review & editing (equal). **Nathan Arndt:** Methodology (equal). **Zhongrui Li:** Data curation (equal); Formal analysis (equal). **Jungwoo Lee:** Methodology (equal). **Yuchuan Yao:** Methodology (equal). **Susmita Roy:** Data curation (equal); Methodology (equal). **Hillary Cunliffe-Owen:** Data curation (equal); Formal analysis (equal). **Dmitry Reznik:** Methodology (equal). **Chang-Beom Eom:** Conceptualization (equal); Methodology (equal); Supervision (equal).

DATA AVAILABILITY

The data that support the findings of this study are available within the article.

REFERENCES

[1]W. Rauch, H. Behner, G. Gieres, B. Sipos, R. Seebock, O. Eibl, R. Kerner, G. Solkner, and E. Gornik, Appl. Phys. Lett. **60**, 3304–3306 (1992).
[2]D. V. Masterov, A. E. Parafin, L. S. Revin, A. V. Chiginev, E. V. Skorokhodov, P. A. Yunin, and A. L. Pankratov, Supercond. Sci. Technol. **30**, 025007 (2017).
[3]L. S. Revin, A. L. Pankratov, D. V. Masterov, A. E. Parafin, S. A. Pavlov, A. V. Chiginev, and E. V. Skorokhodov, IEEE Trans. Appl. Supercond. **28**, 1 (2018).
[4]R. Tsuchiya, M. Kawasaki, H. Kubota, J. Nishino, H. Sato, H. Akoh, and H. Koinuma, Appl. Phys. Lett. **78**, 790–792 (2001).
[5]U. Welp, K. Kadowaki, and R. Kleiner, Nat. Photonics **7**, 702–710 (2013).
[6]D. Stornaiuolo, G. Papari, N. Cennamo, F. Carillo, L. Longobardi, D. Massarotti, A. Barone, and F. Tafuri, Supercond. Sci. and Technol. **24**, 045008 (2011).
[7]C. Seo, J. Kim, S. Eom, K. Kim, and H. Ryeol Park, J. Korean Phys. Soc. **81**, 490–501 (2022).
[8]K. Wan, A. K. Jain, and J. E. Lukens, "Submillimeter wave generation using Josephson junction arrays," Appl. Phys. Lett. **54**, 1805–1807 (1989).
[9]A. K. Jain, P. Mankiewich, and J. E. Lukens, "Observation of phase coherence among multiple Josephson oscillators," Appl. Phys. Lett. **36**, 774–776 (1980).
[10]L. S. Revin, D. V. Masterov, A. E. Parafin, S. A. Pavlov, D. A. Pimanov, A. V. Chiginev, A. V. Blagodatkin, I. V. Rakut', E. V. Skorokhodov, A. V. Gordeeva, and A. L. Pankeratov, "A bunch of YBCO Josephson generators for the analysis of resonant cold-electron bolometers," Appl. Sci. **12**(23), 11960 (2022).
[11]C. Peroz and A. F. Degardin, J.-C. Villegier, and A. J. Kreisler, "Fabrication and characterization of ultrathin PBCO/YBCO/PBCO constrictions for Hot electron bolometer THz mixing application," IEEE Trans. Appl. Supercond. **17**(2), 637–640 (2007).
[12]S. Macis, M. C. Paolozzi, A. D'Arco, L. Tomarchio, A. Di Gaspare, and S. Lupi, Appl. Sci. **12**, 10242 (2022).
[13]E. Färber, N. Bachar, H. Castro, E. Zhukova, and B. Gorshunov, "Ca doped YBCO films in THz frequency range," J. Phys. Conf. Ser. **400**, 022018 (2012).
[14]M. Tonouchi, M. Tani, Z. Wang, K. Sakai, M. Hangyo, N. Wada, and Y. Murakami, "Enhanced THz radiation from YBCO thin film bow-tie antennas with hyper-hemispherical MgO lens," IEEE Trans. Appl. Supercond. **7**(2), 2913–2916 (1997).

01 April 2024 20:16:50

© Author(s) 2024

[15]M. Yu, H. Geng, T. Hua, D. An, W. Xu, Z. N. Chen, J. Chen, H. Wang, and P. Wu, "Series YBCO grain boundary Josephson junctions as a terahertz harmonic mixer," Supercond. Sci. Technol. **33**, 025001 (2020).
[16]J. Keller, G. Scalari, F. Appugliese, E. Mavrona, S. Rajabali, M. J. Süess, M. Beck, and J. Faist, "High T_c superconducting THz metamaterial for ultrastrong coupling in a magnetic field," ACS Photonics **5**(10), 3977–3983 (2018).
[17]J. Gao, Y. Bogulavskij, B. Klopman, G. Gerritsma, and H. Rogalla, Appl. Phys. Lett. **59**, 2754 (1991).
[18]J. Barner, C. T. Rogers, A. Inam, R. Ramesh, and S. Bersey, Appl. Phys. Lett. **59**, 742 (1991).
[19]M. A. Sato, T. Gustavo, K. Utagawa, and T. Morishita, Jpn. J. Appl. Phys. **41**, 5572 (2002).
[20]I. H. Song, E.-H. Lee, B. M. Kim, I. Song, and G. Park, Appl. Phys. Lett. **74**, 2053–2055 (1999).
[21]M. A. J. Verhoeven, G. J. Gerritsma, H. Rogalla, and A. A. Golubov, Appl. Phys. Lett. **69**, 848–850 (1996).
[22]K. Verbist, O. I. Lebedev, G. Van Tendeloo, M. A. J. Verhoeven, A. J. H. M. Rijnders, D. H. Blank, and H. Rogalla, Appl. Phys. Lett. **70**, 1167 (1997).
[23]H. Kandel, T. P. Chen, M. Iliev, S. Bourdo, F. Watanabe, H. W. Seo, and T. Vishwanathan, Appl. Phys. Lett. **100**, 252601 (2012).
[24]I. Takeuchi *et al.*, Appl. Phys. Lett. **69**, 112 (1996).
[25]J. M. Cowley, *Electron Diffraction Techniques* (Oxford Science Publications, 1992), ISBN: 978-0198555582.
[26]Z. (Jerry) Li, *Advances in X-ray Absorption Fine Structure Analysis* (Central West Publishing, 2020), ISBN 978-1-925823882.
[27]E. Olsson, A. Gupta, M. D. Thoules, A. Segmuller, and D. R. Clarke, Appl. Phys. Lett. **58**, 1682–1684 (1991).
[28]J. Z. Wu, P. Y. Hsieh, A. V. McGuire, D. L. Schmidt, L. T. Wood, Y. Shen, and W. K. Chu, Phys. Rev. B **44**, 12643 (1991).
[29]I. E. Trofimov, A. P. Litvinchuk, K. Kamarfis, and C. Thomsen, and H.-U. Habermeier," J. Supercond. **7**(1), 209–211 (1994).
[30]H.-U. Habermeier, A. A. C. S. Lourenqo, B. Friedl, J. Kircher, and J. Köhler, Solid State Commun. **77**(9), 683–687 (1991).
[31]A. Cassinese, A. Di Chiara, F. Miletto Granozio, S. Saiello, U. Scotti di Uccio, and M. Valentino, "Morphological and structural properties of high-quality YBCO films," J. Mater. Res. **10**, 11 (1995).
[32]C. R. Hunt, D. Nicoletti, S. Kaiser, D. Propper, T. Loew, J. Porras, B. Keimer, and A. Cavalleri, Phys. Rev. B **94**, 224303 (2016).
[33]T. Uchiyama and I. Iguchi, "Control of crystal orientation in YBCO thin films by an oxygen diffusion process," Supercond. Sci. Technol. **17**, 592 (2004).
[34]H. Kandel, T. P. Chen, M. Iliev, S. Bourdo, F. Watanabe, H. W. Seo, and T. Vishwanathan, "Electrical transport and Raman spectral studies of (110)-oriented $PrBa_2$ $(Cu_{0.8}M_{0.2})_3O_7$ (M = Ga, Al, Zn, Ni) thin films," J. Appl. Phys. **113**, 143710 (2013).
[35]H. Kandel, M. Iliev, N. Arndt, and T. P. Chen, Adv. Mater. Sci. Eng. **2020**, 5937494.
[36]C. Thomsen, A. P. Litvinchuk, E. Schonherr, and M. Cardona, Phys. Rev. B **45**, 8154–8157 (1992).
[37]P. Zhao, X. Ouyang, J. Yu, H. Xu, S. Wang, and F. Li, "Measurement of residual stress in YBCO thin films by Raman spectroscopy," J. Low Temp. Phys. **202**, 382–396 (2021).
[38]A. Inam *et al.*, Appl. Phys. Lett. **57**, 2484 (1990).
[39]T. Terashima, Y. Bando, K. Iijima, K. Yamamoto, and K. Hirata, Appl. Phys. Lett. **53**, 2232 (1988).
[40]W. K. Chu *et al.*, Appl. Phys. Lett. **72**, 246–248 (1998).
[41]Y. Uzun, O. Kuran, and I. Avci, J. Supercond. Novel Magn. **30**, 2335–2340 (2017).
[42]S. A. Zhgoon, G. D. Lobov, Y. V. Kislinskii, A. R. Kuzhakhmetov, and E. A. Stepantsov, "Phase locking up to 2.5 THz in grain-boundary Josephson junctions at 77 K," Appl. Supercond. **3**(1–12), 615–619 (1995).

01 April 2024 20:16:50

© Author(s) 2024